ELSEVIER

Solid State Ionics 147 (2002) 13–22

SOLID STATE IONICS

www.elsevier.com/locate/ssi

Electrochemical study of the SnO_2 lithium-insertion anode using microperturbation techniques

Chunsheng Wang [a,*], A. John Appleby [a], Frank E. Little [b]

[a] *Center for Electrochemical Systems and Hydrogen Research, Texas Engineering Experiment Station, Texas A&M University, 238 Wisenbaker, 3402 TAMU, College Station, TX, 77843-3402, USA*

[b] *Center for Space Power, Texas Engineering Experiment Station, Texas A&M University, College Station, TX, 77843-3118, USA*

Received 3 October 2001; received in revised form 19 December 2001; accepted 21 December 2001

Abstract

A disk pressed from commercial SnO_2 powder, sandwiched between two nickel screen current collectors, was used as a lithium-ion secondary anode. Its electrochemical lithium insertion–extraction behavior was investigated by galvanostatic charge–discharge and galvanostatic intermittent titration (GITT) using a microcurrent on one current collector. The trans-electrode voltage was measured to monitor the transmissive resistance across the SnO_2 electrode during the discharge–charge process. Special electrochemical impedance spectroscopy (EIS) protocols were used to investigate the kinetic and transmissive impedances during initial lithium insertion. Protocol B or C EIS, described in the text, give the local transmissive impedance near the operating current collector, while Protocol B′ or C′ give the local transmissive impedance near the other current collector. The use of special EIS protocols showed that the inner transmissive impedance near the operating current collector side is higher than that near the other current collector.

Keywords: SnO_2 anode; Special electrochemical impedance spectroscopy; Galvanostic intermittent titration (GIT)

1. Introduction

Tin oxide-based compounds are attractive as insertion anodes for lithium-ion cells because of their higher energy densities than those of carbonaceous electrodes [1]. A simple two-step reaction mechanism for tin oxide-based compounds with lithium has been proposed [2,3]. In the initial lithium reaction, SnO_2 irreversibly decomposes to Sn(II) oxide and then forms metallic tin [4] and a Li_2O matrix [5], followed by subsequent reversible Li–Sn alloying–dealloying.

Initially, the SnO_2 electrode is an n-type semiconductor [6]. During initial Li insertion, the electronic insulator and a Li^+-conducting solid electrolyte Li_2O containing nano-sized tin particles is formed [7]. If the tin particle-to-particle distance is within the length for high-probability electron tunneling, the electrochemical reaction will take place on the electrode surface. Otherwise, the charge-transfer reaction will take place at the Sn/Li_2O electrolyte interface inside the electrode structure. Hence, Sn nano-particles located at distances beyond the electron tunneling length from other Sn nano-particles, or from the

* Corresponding author. Tel.: +1-979-845-8281; fax: +1-979-845-9287.

E-mail address: cswang@tamu.edu (C. Wang).

0167-2738/02/$ - see front matter
PII: S0167-2738(02)00041-3

current collector, will be electrochemically inaccessible for Li insertion. Therefore, the electronic contact resistance [8–12] of the SnO_2 electrode is a sensitive indicator of its electrochemical performance.

The relative change in conductivity of SnO_2 during cyclic voltammetry between 2.5 and 0 V vs. Li was measured by Mohamedi and co-workers [13] using the interdigitated array electrode (IDA). An order of magnitude change in conductivity was observed over this potential range due to the transformation of SnO_2 to Li_2O and Li–Sn alloy.

Electrochemical impedance spectroscopy (EIS) is a powerful tool for both reaction kinetics and transmissive (or intrinsic) impedance measurement [8–12], because it can give individual resistances for each reaction step if their time constants are resolvable. Much EIS work has been carried out on measuring the kinetic parameters of the Li–SnO_2 electrode [13–15]. However, these EIS results show wide variations, because the intrinsic impedance changes more than 10-fold during Li insertion–extraction, and it is in series with the reaction impedance.

In this paper, special EIS protocols and galvanostatic intermittent titration (GITT) using intermittent microcurrent were applied on sandwiched SnO_2 powder electrodes to investigate the kinetics and transmissive resistance change during Li insertion–extraction cycles. The voltage across the sandwiched SnO_2 electrode was monitored to evaluate the relative change in conductivity.

2. Experimental

2.1. Cell preparation and electrochemical measurements

Composite SnO_2 electrodes were prepared from a mixture of 80:10:10 wt.% SnO_2 powder (Aldrich Chemical), carbon black and pure polyvinylidene fluoride between two nickel screen current collectors using 1-methy1-2-pyrrolidinone as solvent. After drying at 120 °C for 10 h, the electrodes were pressed into a sandwich structure with a diameter of about 1.0 cm, and thickness 0.1 cm, typically containing 100–120 mg of active SnO_2. A rather thick electrode was chosen to prevent contact between the two Ni meshes. The configuration of typical electrodes has been shown in previous papers [8–12]. To simulate the real conditions of a Li-ion cell, the Ni sandwiched SnO_2 electrode was wrapped with a Celgard 2400 separator and then compressed between two PTFE holders with small holes to allow penetration of electrolyte. Electrochemical measurements were conducted in a special three-electrode PTFE cell with two lithium foils as both counter and reference electrodes, with an electrolyte consisting of 1.0 M $LiPF_6$ in 1:1:3 by volume mixture of ethylene carbonate (EC)–propylene carbonate (PC)–dimethylcarbonate (DMC) (High-Purity Lithium Battery Grade, Mitsubishi Chemical). The electrodes were discharged (Li insertion) and charged (Li extraction) on one side only (W_1 side in Fig. 1) using an Arbin (College Station, TX) automatic battery cycler, and the voltage differences across both sides were used to monitor their relative conductivity change.

2.2. GITT measurements

Lithium was inserted into or extracted from the SnO_2 electrode in a series of intermittent discharge or charge steps at 7.0 mA/g for 1.0 h with the electrode at open circuit for 1.5 h between each step to establish a pseudo-equilibrium condition. Meanwhile, the voltage across the SnO_2 electrode was recorded by computerized data acquisition. The voltage difference across the electrode without the influence of electrochemical charge–discharge overpotential can be obtained using GITT measurements.

2.3. EIS measurement

Electrochemical impedances were measured from 65 kHz to 1.0 MHz at 5 mV potentiostatic signal amplitude, using a Solartron FRA 1250 frequency response analyzer and a Solartron model 1286 electrochemical interface. Six EIS protocol measurements (Protocols A, B, B′, C, C′ and D) were performed after a rest period of 10 h during each series of galvanostatic discharge processes, the current being applied to on by one side of the freshly prepared SnO_2 electrodes. The potentials at each side of the electrode were recorded before and after each galvanostatic current interruption. Two new transmissive impedance protocols (Protocols B′ and C′) using modified Solartron electrochemical interface terminal-to-electrode connections were carried out, together with four EIS protocols previously used (Pro-

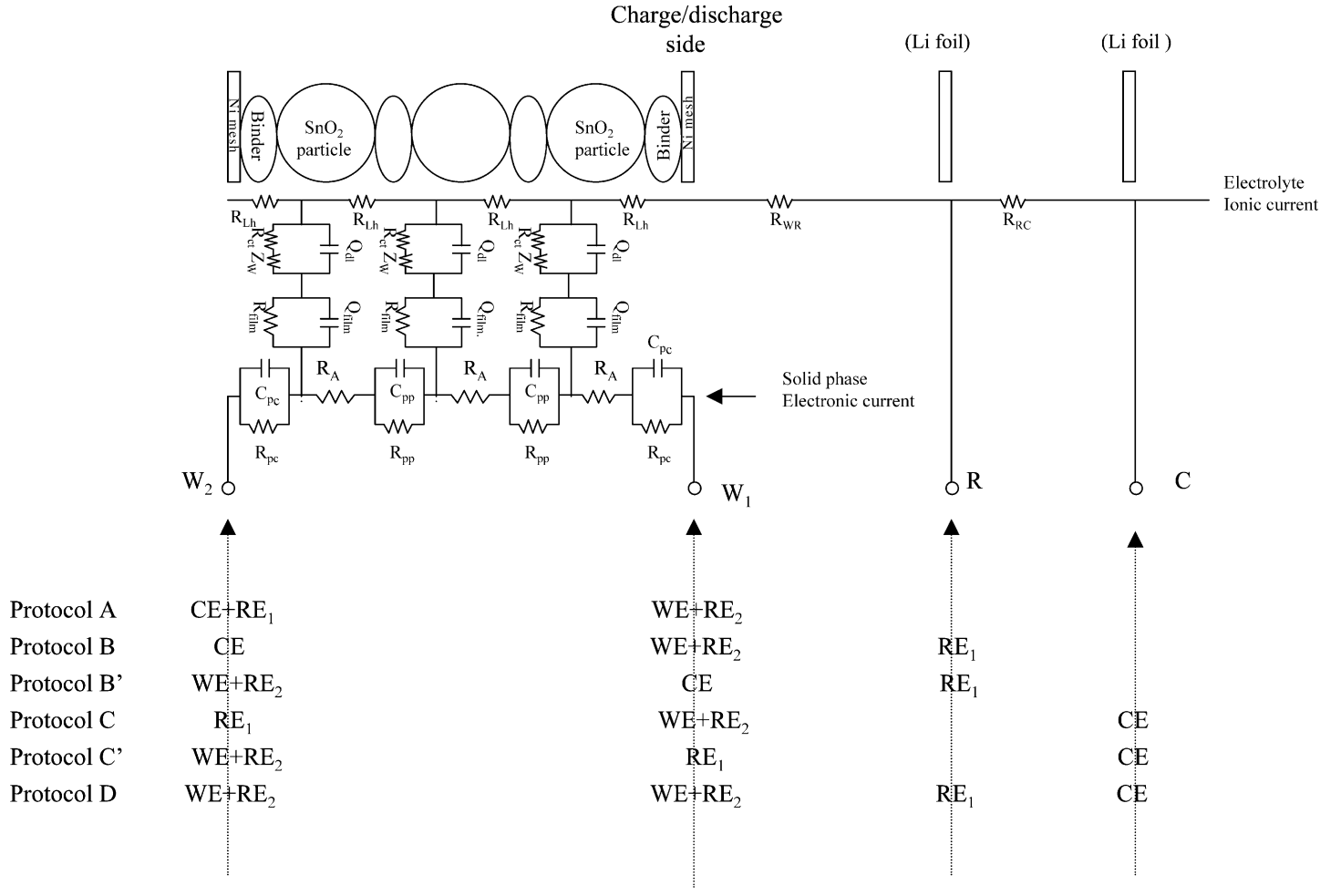

Fig. 1. Schematic diagram of cell with porous ion insertion anode and special Solatron electrochemical interface terminal-to-electrode connections. The transmission line equivalent circuit for ion insertion–extraction into the active anode is also shown. R_A, R_{Lh}, R_{WR}, and R_{RC}: electronic resistance of active particle; ion resistance of electrolyte in pores; reference electrode to working electrode ionic resistance; and reference electrode to counter electrode ionic resistance. R_{pc}, R_{pp}, R_{film} and R_{ct}: active particles-to-current collector; particles-to-particles; SEI film; and charge-transfer resistances. C_{pc} and C_{pp}: particle-to-current collector and particle-to-particle contact capacitances. Q_{film} and Q_{dl}: constant-phase elements for the film and for the double-layer respectively. Z_W: finite Warburg element for lithium in electrode.

tocol A, B, C, and D) [10,16]. The latter are shown again in Fig. 1 for clarity. The physical meanings of the six EIS protocols may be summarized as follows.

Protocol A gives the transmissive impedance of the SnO_2 anode, including the electronic impedance of the SnO_2 particles, various contact impedances (particle-to-particle and particle-to-current collector) with some contribution from electrochemical (Faradaic) reaction when the intrinsic resistance is large. Protocol B gives the transmissive impedance in series with the reaction impedance, including the transmissive impedance near the charging side (W_1) of the SnO_2 anode. Similarly, Protocol B′ reflects the transmissive impedance near the non-charging (W_2) side of the electrode. Protocol C and C′ are the same as Protocol B and B′, respectively. Protocol D gives the electrochemical reaction impedance of the anode using both current collectors.

3. Results and discussion

3.1. Discharge–charge behavior of the SnO_2 anode

Fig. 2 shows the potential of the operating current collector, that of the unconnected current-collector, and the trans-electrode voltage for the SnO_2 anode on the 1st, 3rd and 11th cycles. The initial Li-insertion capacity and potential curve are similar to those reported by Courtney and Dahn [2] for a commercial SnO_2 sample, but the Li-extraction capacity is smaller than theirs. A possible reason for this is the greater thickness of the Ni mesh sandwich anode used here (1.0 mm compared with 0.125 mm) [2]. For initial discharge (Li insertion), the voltage pseudo-plateau at around 1.0 V (~400 mA h/g) may be interpreted as the reduction of Sn^{IV} to a mixed valence Sn^{II} [17], and the gradual decrease in potential (>0.4–0.6 V) as a further reduction of Sn^{II} to Sn^0. The sloping potential plateau below 0.4 V represents Li–Sn alloy formation. The trans-electrode voltage change during Li insertion–extraction can be used to monitor the relative change in conductivity if the change in electrochemical charge–discharge polarization is small [11]. The trans-electrode voltage first increased during the stepwise reduction of Sn^{IV} to mixed valence Sn^{II} and Sn^0 (>0.6 V), and then began to decrease during further reduction to Sn^0. It decreased further following Li_xSn alloy formation because of the increase in the compression of the anode resulting from the expansion of Li_xSn as it forms in the PTFE fixture. Expansion during Li alloying with Sn has been confirmed by in situ atomic force and optical microscopy observations on Li insertion–extraction in and from a SiSn film [18]. It seems difficult to attribute the increase in trans-electrode voltage occurring below 0.2 V only to pulverization of the $Li_{4.4}Sn$ alloy [11]. This is because the low conductivity during the first cycle resulting from $Li_{4.4}Sn$ pulverization should then decrease further due to shrinkage during the corresponding initial Li extraction and that in subsequent Li insertion–extraction cycles. However, below 0.2 V the trans-electrode voltage changes (Fig. 2) are almost reversible during these cycles. The figures also show that the trans-electrode voltage grdually increased during discharge–charge cycles. At the same time, the Li extraction capacity quickly decreased from 234 mA h/g on the first cycle to 117 mA h/g on the 11th cycle. Therefore, the decline in capacity of the anode may largely be attributed to a decrease in the number of active Sn particles and in the number of effective electronic contacts between active Sn particles and the Li_2O matrix. Trans-electrode voltage profiles during each cycle are similar to the conductivity changes reported by Mohamedi using the IDA SnO_2 electrode referred to earlier [13], and are different from those for non-compressed SnO_2 [11].

To avoid the influence of electrochemical polarization on the trans-electrode voltage, galvanostatic intermittent titration (GITT) measurements were applied to one current collector on the 4th cycle (Fig. 3). The results show that the open-circuit potentials at both sides of the SnO_2 anode are almost the same at Li-insertion potentials above 0.25 V and at Li-extraction potentials below 0.45 V. After this, the open-circuit trans-electrode voltage increases at Li insertion potentials below about 0.25 V and Li extraction potentials above 0.45 V. The trans-electrode voltage peak around 0.5 V during Li insertion (Fig. 3) is largely related to electrode polarization. However, the high trans-electrode voltage during Li insertion below 0.25 V and in Li extraction above 0.45 V result from the low electrode conductivity. A possible reason for a low conductivity below 0.25 V is the disappearance of the electronically conductive Sn–O interaction [17], which is replaced by independent domains of electronically insulating Li_2O matrix and Li–Sn alloy particles. The high trans-electrode voltage at Li-extraction potentials above 0.6 V may be attributed to poor contact between the Sn particles and

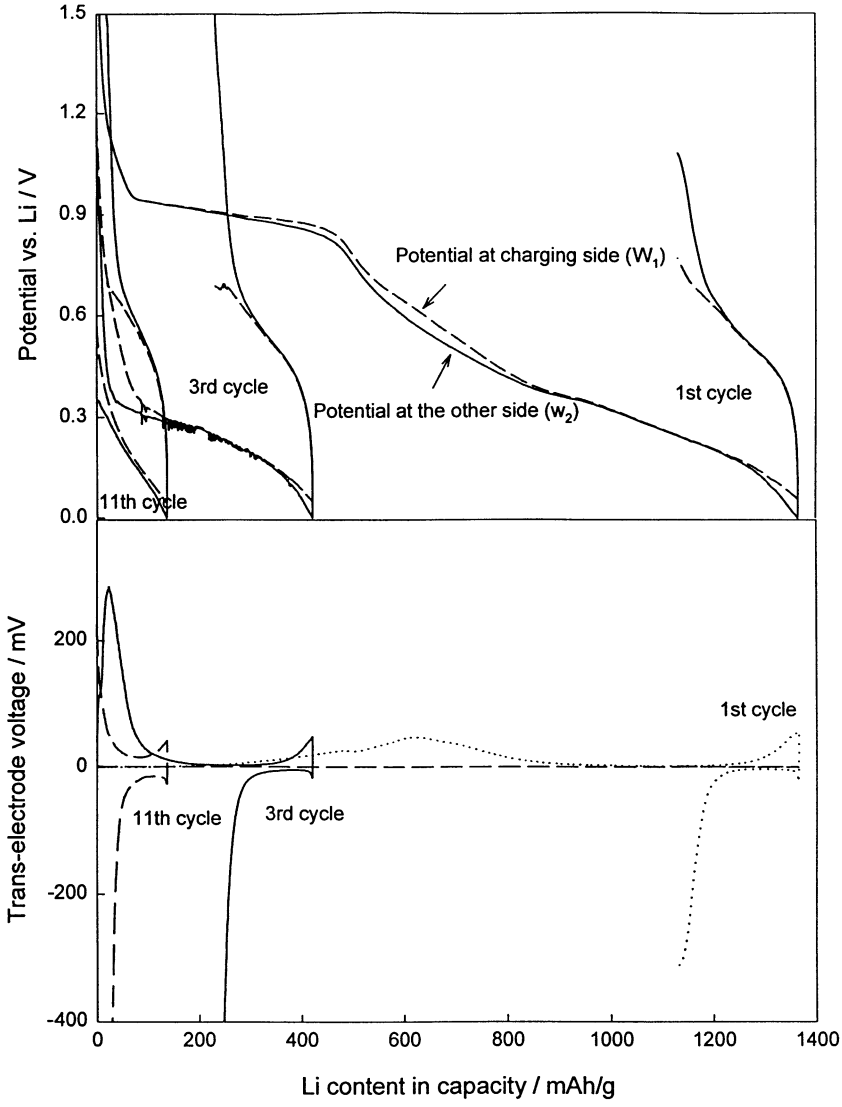

Fig. 2. Potential on the charge–discharge W_1 side, on the W_2 side and the transelectrode voltage for compressed SnO_2 anode on the 1st, 3rd and 11th Li insertion–extraction cycles at 2.0 mA/g current. The Ni-sandwiched SnO_2 electrode was wrapped in a Celgard 2400 separator and then compressed between two PTFE holders with small holes to allow penetration of electrolytes.

the Li_2O matrix, which results in high electrochemical polarization and low electrical conductivity.

3.2. Reaction kinetic and transmissive impedance measurement during the initial Li insertion into the SnO_2 anode

Fig. 4 shows the potentials on the electrically connected and unconnected sides of the anode at the end of each intermittent discharge (2.0 mA/g for different times) and after 10-h relaxation between each intermittent discharge as a function of discharge capacity. After this relaxation, the special protocol EIS scans shown in Fig. 1 were applied to determine the kinetic and transmissive impedances for initial lithium insertion. The kinetic and transmissive impedances using Protocol D and Protocol A in Fig. 1 are shown in Fig. 5. The trans-electrode voltage profile of the SnO_2 elec-

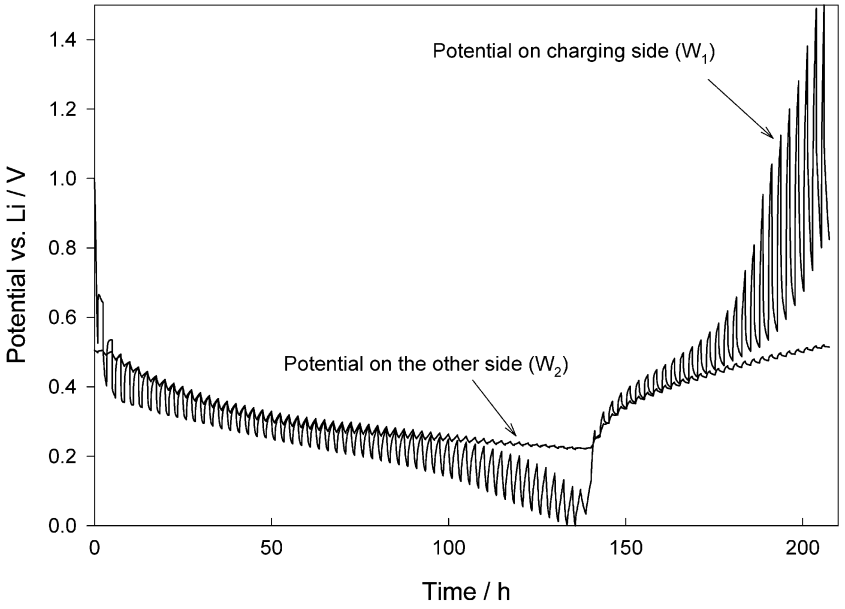

Fig. 3. Potential at charge–discharge W_1 side and on W_2 side as a function of time for the 4th cycle of compressed SnO_2 anode using galvanostatic intermittent titration via applied microcurrent (GITT) technique. Charge–discharge current: 7.0 mA/g. The intermittent current was applied for 1.0 h then switched off for 1.5 h.

trode under a galvanostatic intermittent discharge and under special protocol EIS scans (Fig. 4) was similar to the trans-electrode voltage change under continuous galvanostatic charging (Fig. 2), except below 0.6 V. Under these conditions, the trans-electrode voltage under continuous charge begins to decrease, but remains stable for the intermittent discharge and EIS scan sample. This difference may be due to a lower compression in the PTFE fixture for the EIS scan anode or by a change in electrode state resulting from the special EIS scans. During reduction of SnO_2 and during Li–Sn alloy formation, the open-circuit potential after 10 h relaxation returns to the SnO_2 reduction potential until the potential on the charge side is below 0.2 V and then begins to decrease (Fig. 4). This result suggests that the initial reduction of SnO_2 is not complete until 0.2 V, which is in agreement with a recent study on SnO_2 reduction using X-ray absorption, ^{119}Sn Mössbauer spectroscopy, and X-ray diffraction [17].

At open-circuit potential, the reaction kinetic impedance (Fig. 5a) shows a depressed high-frequency semicircle along with a steep line at low frequencies. With lithium insertion from 1.0 to 0.4 V, a new semicircle appears in the high frequency region and its diameter increases with Li insertion. The possible reason is (i) the formation and growth of a solid electrolytes interphase (SEI) film on the SnO_2 surface and (ii) reduction of the semi-conductive SnO_2 to form Sn dispersed within an electronically insulating Li_2O matrix because the performance of Li-ion electrolyte Li_2O is similar to that of an SEI film. On further Li insertion, the diameters of both semicircles increased (especially at potentials below 0.2 V), which is attributed to (i) particle pulverization, resulting in increasing transmissive impedance in series with the kinetic impedance, (ii) SEI film formation on the new surface induced by the pulverization of Li_xSn alloy, (iii) disappearance of the Sn–O interaction below 0.2 V.

The transmissive impedance at open-circuit potential shows two semicircles (Fig. 5b), which may be respectively attributed to SnO_2 particle-to-current collector and particle-to-particle impedances. With lithium insertion, the real part of the transmissive impedance first decreases rapidly, and then began to increase gradually. The increase in transmissive impedance may be attributed to (i) the growth of electronically insulating Li_2O between Sn particles and in the Sn particle-to-current collector interface, (ii) Pul-

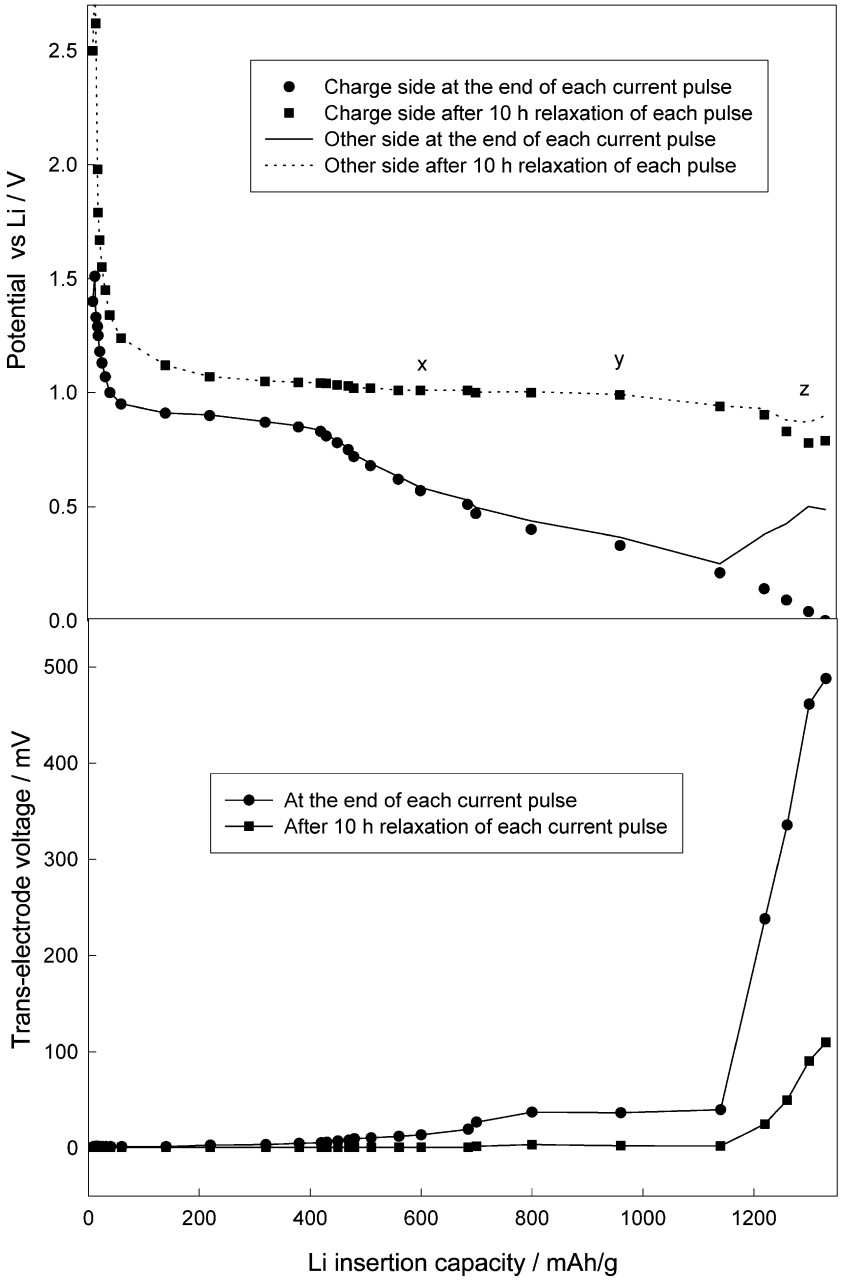

Fig. 4. Potentials on discharge and non-discharging side of SnO_2 anode at the end of each intermittent discharge (2.0 mA/g for different times) and after 10-h relaxation between each intermittent discharge as a function of charge capacity. The special protocol EIS scans shown in Fig. 1 were applied to the SnO_2 anode at the potential reached after 10-h relaxation between each intermittent discharge to determine the kinetic and transmissive impedances for initial lithium insertion.

verization and disappearance of the Sn–O interaction. The gradual disappearance of the Sn–O interaction (or partial pulverization) increases the second semicircle of the transmissive impedance more rapidly, so gradually the second semicircle becomes a sloping line at potentials below 0.2 V. Since part of the transmissive

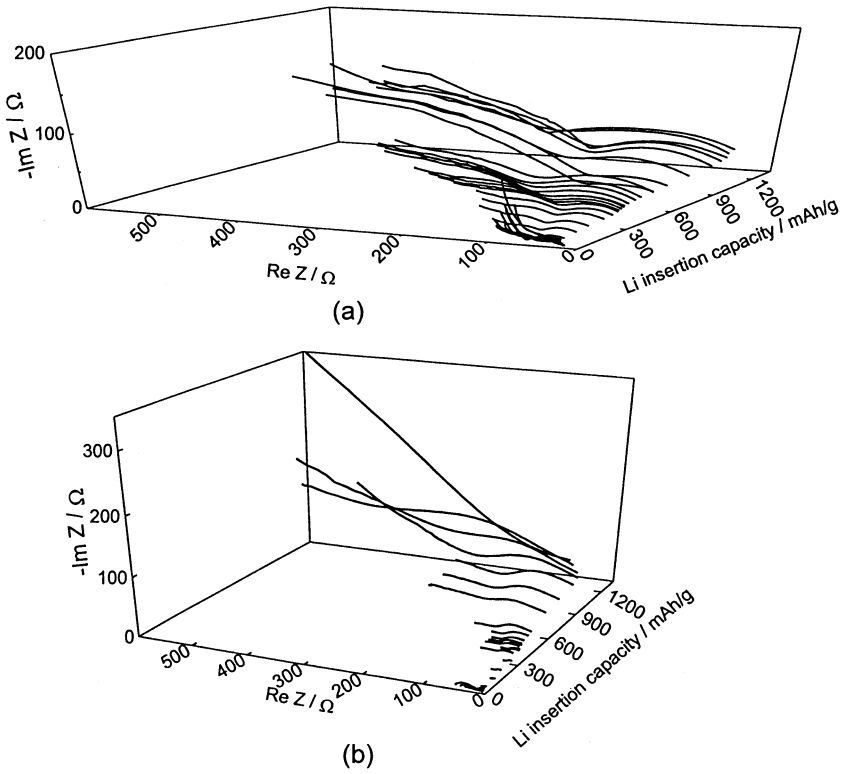

Fig. 5. Nyquist plots for (a) reaction kinetics (Protocol D) and (b) transmissive impedance (Protocol A) measured at different initial Li insertion levels (following 10-h relaxation between each intermittent discharge).

impedance is in series with the kinetic impedance [9, 10] and the transmissive impedance is large, especially at high Li content (Fig. 5b), the kinetic parameters obtained directly from the normal EIS (Protocol D) are not reliable.

3.3. Local transmissive impedance measurements on the SnO_2 anode

As already stated, the SnO_2 electrode was discharged by Li insertion only on one side. During initial discharge from 2.7 V to 0.2 V (Fig. 4), the trans-electrode voltage after relaxation for 10.0 h remained almost zero. However, the trans-electrode voltage in the intermittent discharge process gradually increased. It is reasonable to believe that the state of charge (SOC) of SnO_2 particles differs according to their position in the electrode. Further, SEI film formation at different locations away from the charging current collector (W_1) is different [19] due to spatial variations of the current density. These factors will result in a different transmissive impedance across the electrode. The transmissive impedance measured using Protocol A can give the total particle-to-current collector and particle-to-particle contact impedance, while the transmissive impedance measured using Protocols B and C can give the transmissive impedance of the side close to the charging side of the electrode (the W_1 side). Similarly, the Protocols B′ and C′ spectra on the non-charging side should give the transmissive impedance close to this side (the W_2 side). Therefore, the transmissive impedance using Protocol B (or C) plus Protocol B′ (or C′) will be equal to the transmissive impedance using Protocol A. Fig. 6 shows the transmissive impedances measured using Protocols A, B, B′ C, and C′ at discharge levels specified at the *x*, *y*, and *z* points in Fig. 4. The results shown in Fig. 6 may be summarized as follows.

(1) At the two Li insertion levels *x* and *y* (Fig. 6a and b), the parallel resistance of the first semicircle is larger than that of the second semicircle for the transmissive

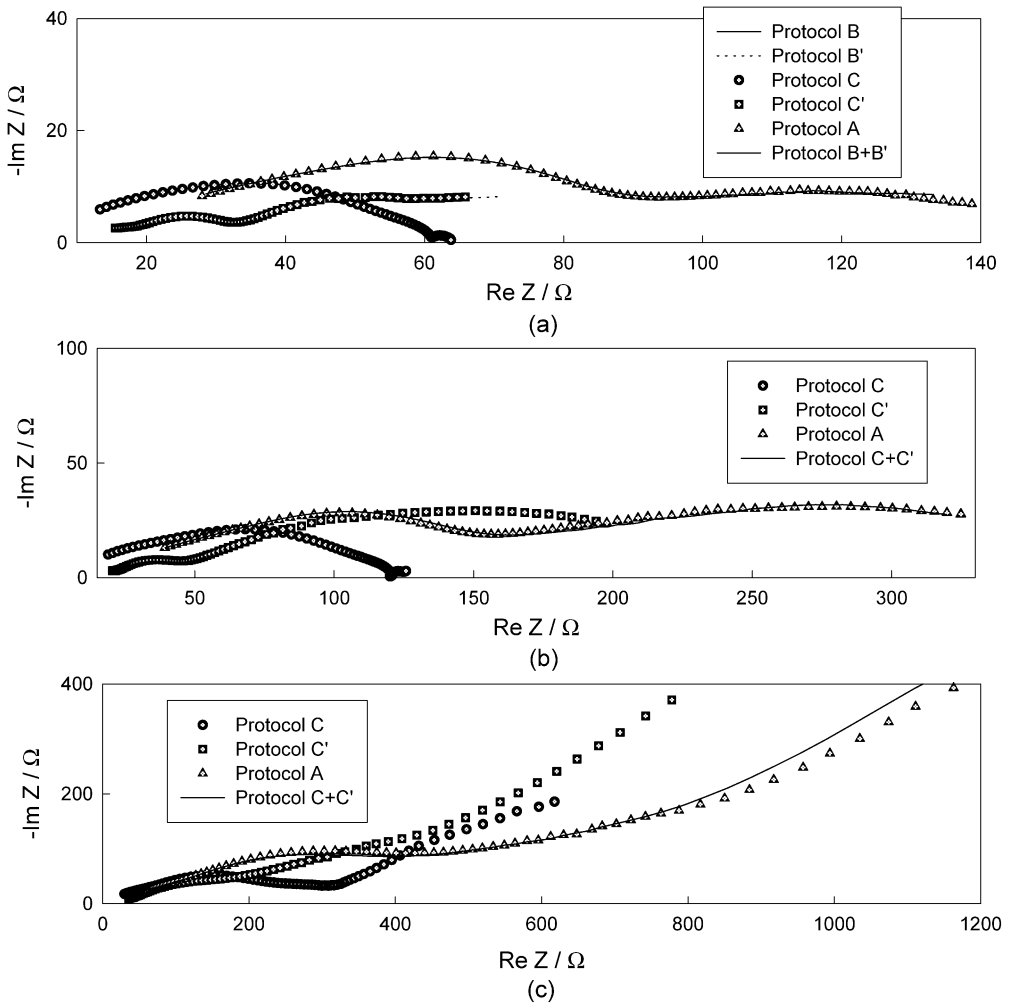

Fig. 6. The transmissive impedances using Protocols A, B, B′ C, and C′ at Li insertion levels given at the (a) *x*, (b) *y* and (c) *z* points specified in Fig. 4.

impedance using either Protocol B or C. In contrast, the parallel resistance of the first semicircle diameter is smaller than the second for Protocol B′ and C′ . This indicates that transmissive resistance (including the electronic contact resistance and part of ionic reaction resistance) near the charging current side (W_1) is higher than that near the other side (W_2). Similar results were also reported by Zhang et al. [19], who found that the SEI layer changes its location relative to the current collector [19].

(2) At Li insertion level z (potentials below 0.2 V), both sides of the SnO_2 anode become insulating. The second semicircles in Protocol C and C′ then becomes a sloping line as described earlier. The parallel resistance of the first semicircle as measured on the charged current collector side is still larger than that on the other side (Fig. 6c).

(3) In Fig. 6a, the Protocol B and B′ EIS are the same as those for Protocols C and C′, in agreement with previous results [10,16]. As expected, the impedance measured at *x*, *y* and *z* points using A is equal to the sum of the impedances using Protocol C and C′. Therefore, impedance measurement using Protocols B (or C), and B′ (or C′) are powerful methods for ob-

taining impedance information in the interior of the electrode near to the charging and non-charging current collectors, respectively.

4. Conclusions

Galvanostatic discharge–charge and galvanostatic intermittent titration using microcurrent (GITT) were applied to one side of SnO_2 electrodes sandwiched between nickel current collectors. Special electrochemical impedance spectroscopy (EIS) protocols were used to measure the reaction kinetic and transmissive impedances during initial Li insertion into the SnO_2 anode. The trans-electrode voltage measured at different Li insertion levels show that semiconducting SnO_2 is replaced gradually by electronically insulating Li_2O during the reaction $4Li + SnO_2 \rightarrow 2Li_2O + Sn$, which results in an increasing transmissive impedance. Since the intrinsic impedance is partially in series with the kinetic impedance, and since a large intrinsic impedance exists during charge–discharge of the SnO_2 electrode, reliable kinetic parameters cannot be obtained from normal EIS measurements, such as Protocol D. The use of special EIS protocols showed that the inner transmissive impedance near the operating current collector side is higher than that near the other current collector.

References

[1] Y. Idota, A. Matsufuji, Y. Maekawa, M. Miyaki, Science 276 (1997) 1395.
[2] I.A. Courtney, J.R. Dahn, J. Electrochem. Soc. 144 (1997) 2045.
[3] I.A. Courtney, J.R. Dahn, J. Electrochem. Soc. 144 (1997) 2943.
[4] N. Li, C.R. Martin, B. Scrosati, Electrochem. Solid-State Lett. 3 (2000) 316.
[5] I.A. Courtney, R.A. Dunlap, J.R. Dahn, Electrochim. Acta 144 (1997) 2943.
[6] J. Morales, L. Sanchez, J. Electrochem. Soc. 146 (1999) 1640.
[7] R. Huggins, J. Power Sources 81 (1999) 13.
[8] C. Wang, I. Kakwan, A.J. Appleby, F.E. Little, J. Electroanal. Chem 489 (2000) 55.
[9] C. Wang, A.J. Appleby, F.E. Little, J. Electroanal. Chem. 497 (2001) 33.
[10] C. Wang, A.J. Appleby, F.E. Little, Electrochim. Acta 46 (2001) 1793.
[11] C. Wang, A.J. Appleby, F.E. Little, J. Power Sources 93 (2001) 175.
[12] C. Wang, A.F. Rakotondrainibe, A.J. Appleby, F.E. Little, J. Electrochem. Soc. 147 (2000) 4432.
[13] M. Mohamedi, S.J. Lee, D. Takahashi, M. Nishizawa, T. Itoh, I. Uchida, Electrochim. Acta 46 (2001) 1161.
[14] H. Li, X. Huang, L. Chen, J. Power Sources 81 (1999) 340.
[15] S. Nam, Y. Kim, W. Cho, B. Cho, H. Chun, K. Yun, Electrochem. Solid-State Lett. 2 (1999) 9.
[16] C. Wang, A.J. Appleby, F.E. Little, J. Electrochem. Soc. 148 (2001) A762.
[17] J. Chouvin, J. Olivier-Fourcade, J.C. Jumasa, B. Simon, Ph. Biensan, F.J. Fernandez Madrigal, J.L. Tirado, C. Perez Vicente, J. Electroanal. Chem. 494 (2000) 136.
[18] L.Y. Beaulieu, K.W. Eberman, R.L. Turner, L.J. Krause, J.R. Dahn, Electrochem. Solid-State Lett. 4 (2001) A137.
[19] X. Zhang, P.N. Ross Jr., R. Kostecki, F. Kong, S. Sloop, J.B. Striebel, K. Striebel, E.J. Cairns, F. McLarnon, J. Electrochem. Soc. 148 (2001) A463.